Extreme Learning Machine-Based Repetitive Proportional Derivative Controller for Robust Tracking and Disturbance Rejection in Rotational Systems

Enggar Banifa Pratiwi [1], Prawito Prajitno [2], Edi Kurniawan [3*]
[1, 2] Departement of Physics, Faculty of Mathematics and Natural Science, Universitas Indonesia, Depok 16424, West Java, Indonesia
[1, 3] Research Center for Photonics, National Research and Innovation Agency, South Tangerang 15314, Banten, Indonesia
Email: [1] enggar.banifa@ui.ac.id, [2] prawito@sci.ui.ac.id, [3] edik004@brin.go.id
*Corresponding Author

Abstract—**Tracking periodic signals and rejecting periodic disturbances are common applications of repetitive control (RC). However, traditional RC methods struggle to compensate for aperiodic disturbances and adapt to system uncertainties, limiting their real-world effectiveness. Existing hybrid approaches often require extensive parameter tuning or suffer from high computational costs, creating a research gap in achieving both adaptability and efficiency. This paper proposes an improved control strategy called extreme learning machine repetitive proportional derivative control (ELMRPDC), which integrates repetitive proportional derivative control (RPDC) with an extreme learning machine (ELM). RPDC ensures accurate tracking of periodic signals, while ELM estimates and compensates for disturbances, enhancing overall performance. Unlike conventional neural network-based controllers, ELM enables rapid adaptation with minimal computational overhead, making it more suitable for real-time applications on resource-constrained systems. The proposed method is analyzed for stability using the Lyapunov approach, ensuring convergence of tracking errors. Extensive simulations are conducted on both rotational and linear dynamic systems under various disturbance conditions, including periodic, time-varying, multi-periodic, and aperiodic disturbances, such as vibration-induced disruptions in machinery. The study also evaluates the impact of hidden layer neuron variations in ELM on disturbance rejection. The best performance is observed for multi-period sinusoidal disturbances, achieving an RMSE of 1.8630 degrees at 1500 neurons, reducing error by 67.47% compared to conventional RPDC. These results highlight ELMRPDC's advantages in computational efficiency, real-time feasibility, and robustness against complex disturbances. The approach holds significant promise for precise reference tracking and disturbance rejection across diverse industrial applications.**

Keywords—Plug-in Repetitive Control; Extreme Learning Machine; Rotational Systems; Periodic Signal Tracking, Multi-Periodic Disturbance Compensation; Aperiodic Disturbance Compensation.

I. INTRODUCTION

Tracking references and rejecting disturbances in the form of repeating signals are common challenges in many control engineering applications. One well-known control approach used to address these issues is repetitive control (RC), which was first introduced by Inoue et al. [1]. This strategy is based on the internal model principle (IMP) [2] and is designed to track periodic signals and/or reject periodic disturbances. RC has been effectively applied in diverse systems for its precise tracking and disturbance rejection, including lower extremity exoskeleton [3], flexible robotic joints [4], piezo-actuated nanopositioning stages [5], piezo-actuated nanoscanners [6], rotational system [7]-[12] bearingless induction motor [13], dynamical galvanometer [14], magnetically suspended rotor system [15], inverters [16]-[20], permanent magnet synchronous motor (PMSM) [21]-[23], electric vehicle charger [24], line-of-sight stabilization [25], electric spring [26], power converters [27], pulsewidth modulation converters [28], minimum and non-minimum phase stabilized plant [29]. Conversely, RC is unable to compensate for non-periodic or aperiodic disturbances, as indicated in [30]-[32]. In addition to being unable to handle aperiodic disturbances, the efficacy of RC is significantly reduced when disturbance period is uncertain or variable, and then the model is subject to nonlinearities and uncertainties [33], [34]. In such cases, the performance of RC deteriorates, resulting in reduced tracking accuracy and system instability. To overcome this challenge, advanced methods are needed to improve the robustness of RC in handling aperiodic disturbances and disturbances with uncertain or time-varying frequencies.

Furthermore, in the majority of rotational systems, the primary issues are nonlinearities such deadzone, backlash, and friction [35]. Ignoring the backlash nonlinearity can affect system performance, introduce unwanted errors, and potentially cause instability or unsatisfactory system performance [36]. In addition to backlash, friction can also result in system instability in addition to a notable decline in tracking performance [37]. Nonlinear friction and backlash have the potential to impair the tracking performance of the control systems and result in energy loss.

According to [38]-[40], several adaptive control strategies have been developed to reduce the uncertainty of nonlinear systems. In [38], presented a novel model-free extended state observer (ESO)-based RC technique aimed at enhancing the rejection of periodic and aperiodic disturbances in control systems. However, the real-time implementation of the ESO may require significant computational resources, especially for systems with high dynamics. In order to compensate for the systems nonlinearities, a linear robust control is designed using the describing function [39], which is ineffective for time-varying friction and backlash.

Neural networks (NN), known for their ability to learn and adapt to complex patterns, can effectively estimate and compensate for different types of disturbances. In [41]-[47], numerous works proposed the integration of control strategies with NN. In [41], proposed an adaptive NN control method that effectively addresses output dead zones in strict-feedback nonlinear systems, ensuring bounded signals and improved stability despite non-smooth nonlinearities. However, the complexity arises from the need to design state observers and implement backstepping techniques, which can lead to longer training durations. In [42], investigated the robust adaptive neuro-fuzzy inference system, which demonstrates efficacy and efficiency in controlling heavy-duty vehicles speed. Nonetheless, there are drawbacks, such as higher complexity and the need for more data to train efficiently. The ELM was initially introduced by Huang et al. [33] in 2006. It consists of a single hidden layer feedforward network (SLFN) and is used in both regression and classification tasks. ELM has gained widespread popularity in various applications due to its simplicity and effectiveness in addressing diverse problems. Standalone ELM has been successfully applied across multiple fields, including power forecasting in photovoltaic systems [48], distributed parameter systems [49], software development effort estimation [50], network intrusion detection [51], multivariant pneumonia classification [52], automated credit scoring [53], transformer fault diagnosis [54], grading diabetic retinopathy [55], non-uniform-intensity light handling [56], electricity consumption series clustering [57], thermostatic bimetal analysis [58], and underground mining [59]. This broad range of applications highlights ELM's adaptability and effectiveness in solving diverse real-world problems [60].

The ELM algorithm is an excellent choice for estimating and compensating for uncertainty, offering advanced drift/shift compensation techniques that enhance both classification accuracy and efficiency. ELM has proven its potential for real-time applications in control systems, offering fast computation and adaptability. It has been successfully applied in various real-time control scenarios, such as steer-by-wire vehicle control [61], hypersonic vehicle control [62], power transmission line deicing robot [63], DC servo motor control [35], sensor drift compensation [64], PMSM [65], bicycle robot [66], electronic throttle [67], variable polarity plasma arc welding [68], inverted pendulum [69], and robot manipulator [70]. The fast nonsingular terminal sliding mode control (SMC)-based strategy for steer-by-wire vehicles uses ELM to estimate the equivalent control in the lower controller, ensuring accurate tracking of the desired front wheel steering angle from the upper controller [61]. For hypersonic vehicles, adaptive laws and learning rates enhance the SMC scheme and ELM-based neural network disturbance observer, enabling precise estimation of unknown disturbances [62]. ELM is also used to compensate for aperiodic disturbances, parameter uncertainties, friction, and backlash in brushless DC servo motors on periodic signals [24]. ELM emerges as a distinct type of NN that offers a simpler architecture and faster learning capability, making it well-suited for real-time control applications [35].

In this study, we aim to integrate ELM with RC to address the limitations of RC, particularly in rejecting non-periodic disturbances. RC is typically limited to rejecting periodic disturbances with fixed, known frequencies. To overcome this, we propose an extreme learning machine repetitive proportional derivative control (ELMRPDC) system for reference tracking and the elimination of various types of disturbances, including periodic, time-varying, multi-periodic, and aperiodic signals. RC is employed for accurate reference signal tracking, while ELM is used to estimate and compensate for the different types of disturbances. ELM is chosen for its simplicity, as it utilizes a single hidden layer feedforward network, eliminating the need for iterative tuning. Unlike traditional neural networks, ELM offers faster computation by randomly assigning input weights and biases, making it highly efficient for real-time applications. The contributions of this work are listed as follows:

- A hybrid control strategy called ELMRPDC is proposed, combining the strengths of RPDC and ELM to enhance simultaneous reference tracking and disturbance rejection in rotational systems.
- The key limitations of RC in handling disturbance rejection of time-varying, multi-periods, and aperiodic signals are addressed by incorporating ELM.
- A stability analysis of the closed-loop system using the proposed ELMRPDC is conducted with Lyapunov approach, ensuring system stability and error convergence.
- The effectiveness of ELMRPDC is demonstrated in several simulation studies, highlighting its superior performance in tracking periodic references and its robustness against various disturbances, compared to standalone RPDC.

The structure of this paper is organized as follows: Section 2 outlines the Methodology, which includes plant modeling, the design of plug-in RC, the design of ELM, and the development of the proposed ELMRPDC control strategy, stability analysis, and robustness analysis. Section 3 provides the simulation results, comparison studies, and the discussion, while Section 4 concludes the study.

II. Method

A. Plant Modelling

The dynamic behavior of the servomotor system can be described by the following differential equation (1) [71].

$$\left(\frac{d}{dt}\omega_l(t)\right)J_{eq} + B_{eq}\omega_l(t) = A_m V_m(t) \tag{1}$$

where $\omega_l(t)$ is load shaft rate, and J_{eq} is the equivalent moment of inertia, B_{eq} is the equivalent viscous damping, A_m is the actuator gain parameter, and $V_m(t)$ is the input voltage. Taking the Laplace transform of (1) and assuming the motor speed $\omega_l(0)$ is initially zero, it yields

$$s\omega_l(s)J_{eq} + B_{eq}\omega_l(s) = A_m V_m(s) \tag{2}$$

Then, the transfer function of the servo system is given by

$$\frac{\omega_l(s)}{V_m(s)} = \frac{A_m}{sJ_{eq} + B_{eq}} \tag{3}$$

which can be rewritten to

$$\frac{\omega_l(s)}{V_m(s)} = \frac{A_m / B_{eq}}{sJ_{eq}/B_{eq} + 1} \tag{4}$$

Using A_m, B_{eq}, J_{eq} parameters to express the steady-state gain K and time constant τ, we have

$$K = \frac{A_m}{B_{eq}} \text{ and } \tau = \frac{J_{eq}}{B_{eq}} \tag{5}$$

Defining the plant output $X(s) = \frac{1}{s}\omega_l(s)$, and $U(s) = V_m(s)$, then (4) can be derived to

$$\frac{X(s)}{U(s)} = \frac{1}{s}\frac{K}{s\tau + 1} \tag{6}$$

Here, $X(s)$ is an angular position as an output, $U(s)$ is an open loop voltage as a control input. Then, performing the Laplace inverse on (6), we get

$$\ddot{x}(t) = -\frac{1}{\tau}\dot{x}(t) + \frac{K}{\tau}u(t) \tag{7}$$

where $x(t)$ is a position output, $\dot{x}(t)$ is a velocity output, $\ddot{x}(t)$ is an acceleration output, $u(t)$ is a control input. We consider that the system (7) is subject to an input disturbance $d_i(t)$, then (7) can be represented by

$$\ddot{x}(t) = -\frac{1}{\tau}\dot{x}(t) + \frac{K}{\tau}[u(t) + d_i(t)] \tag{8}$$

Suppose that $a_0 = -\frac{1}{\tau}$, $b_0 = \frac{K}{\tau}$, then (8) can be rewritten to

$$\ddot{x}(t) = a_0\dot{x}(t) + b_0[u(t) + d_i(t)] \tag{9}$$

$$\ddot{x}(t) = [a_0\dot{x}(t) + b_0 u(t)] + b_0 d_i(t)$$

Thus, the realization of open-loop model (9) is illustrated in Fig. 1.

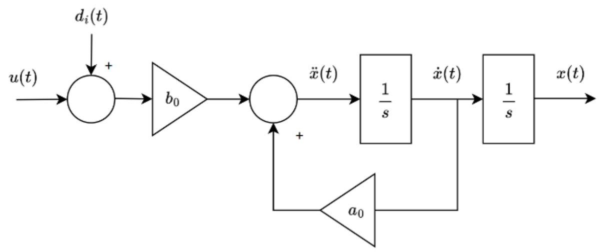

Fig. 1. Open loop plant model with an input disturbance

B. *Design of Plug-in RC (RPDC)*

Plug-in RC refers to the integration of RC with the conventional PD feedback controller, later referred to as RPDC, as shown in Fig. 2. This control strategy is designed to enhance tracking and disturbance rejection for periodic signals and has been applied in programmable AC power sources [72], medical X-ray systems [73], three-phase boost power factor correction rectifiers [74], grid-connected inverters [75], strictly proper plants [76], and two-level grid-connected inverters [77], and grid-tied converter [78]. The RC in RPDC consists of an internal model and a learning function. The internal model acts as a generator of periodic signals for reference tracking or disturbance rejection, while the learning function stabilizes the closed-loop system, typically designed as the inverse of the closed-loop plant model. The internal model of RC is modeled as:

$$\frac{X_R(s)}{E(s)} = \frac{\alpha(s)e^{-sT_R}}{1 - \alpha(s)e^{-sT_R}} \tag{10}$$

where T_R is the period of reference signal, and e^{-sT_R} is a continuous-time delay with the length of T_R, $\alpha(s)$ is a low-pass filter. The low-pass filter $\alpha(s)$ is formulated by,

$$\alpha(s) = \frac{\omega_c}{s + \omega_c}\begin{cases}|\alpha(s)| \approx 1, \omega \leq \omega_c \\ |\alpha(s)| < 1, \omega > \omega_c\end{cases} \tag{11}$$

where ω_c denotes a cut-off frequency. Subtituting (11) to (10), and rearranging, we have

$$X_R(s) - \frac{\omega_c}{s + \omega_c}X_R(s)e^{-sT_R} = \frac{\omega_c}{s + \omega_c}E(s)e^{-sT_R} \tag{12}$$

Multiplying both sides of (12) by $s + \omega_c$, we obtain

$$\begin{aligned} sX_R(s) + \omega_c X_R(s) - \omega_c X_R(s)e^{-sT_R} \\ = \omega_c E(s)e^{-sT_R} \end{aligned} \tag{13}$$

The state-space of the internal model is obtained by performing the inverse Laplace transform on (13), resulting in

$$\begin{aligned} \dot{x}_R(t) = -\omega_c x_R(t) + \omega_c x_R(t - T_R) \\ + \omega_c e(t - T_R) \end{aligned} \tag{14}$$

T_R in (14) is considered part of the predefined assumptions and serves as a fundamental parameter in the design of RC. Assuming the control output of RC is not saturated, the system analysis focuses on the linear response. To assess the accuracy of the system's reference tracking, the tracking error is defined as (15).

$$e(t) = r(t) - x(t) \tag{15}$$

where $r(t)$ is the reference signal.

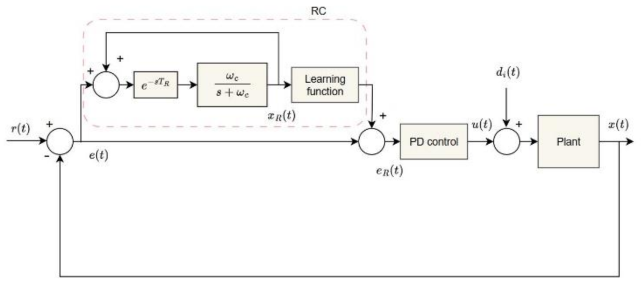

Fig. 2. Block diagram of plug-in RC referred as RPDC

The following assumptions are used in the design of the RPDC controllers.

Assumption 1: The plant parameters K and τ in (8) are assumed to be known, whereas the input disturbance $d_i(t)$ is considered unknown.

Assumption 2: The reference period T_R is assumed to be known and serves as the basis for the design of the RC. Additionally, the bandwidth of the low-pass filter is set to exceed the reference frequency to ensure effective attenuation of high-frequency noise while preserving the desired signal components.

C. Design of Standalone ELM

ELM is a fast and efficient learning algorithm designed for single-layer feedforward networks (SLFNs), where the hidden layer parameters are randomly assigned and the output weights are analytically determined. A standalone ELM has been applied across a wide range of applications. Building upon this foundation, ELM can also be integrated into control systems, where a SLFN is employed as the core structure for this approach. For N arbitrary distinct samples (x_i, τ_i), where $\boldsymbol{x}_i = [x_{i1}\ x_{i2}\ \cdots\ x_{in}]^T \in R^n$ and $\boldsymbol{\tau}_i = [\tau_{i2}\ \tau_{i2}\ \cdots\ \tau_{im}]^T \in R^m$, a standard SLFN incorporating $\widetilde{N}$ hidden-layer neurons is formulated as follows

$$\sum_{i=1}^{\widetilde{N}} \boldsymbol{\beta}_i J(\boldsymbol{x_j}, \gamma_i, \alpha_i) = \boldsymbol{r}_j, \qquad j = 1, \cdots, N \tag{16}$$

where $J(\boldsymbol{x_j}, \gamma_i, \alpha_i)$ is the activation function. The input bias at i −th hidden node is denoted as α_i, and the input weight vector is expressed as $\boldsymbol{\gamma}_i = [\gamma_{i1}\ \gamma_{i2}\ \cdots\ \gamma_{in}]^T$. The output weight vector connecting the i −th hidden node and the output node is described as $\boldsymbol{\beta}_i = [\beta_{i1}\ \beta_{i2}\ \cdots\ \beta_{im}]^T$.

The conventional SLFN, consisting of $\widetilde{N}$ hidden nodes as illustrated in Fig. 3 has the capability to approximate N given samples with a minimal error, denoted as ε. This implies that $\sum_{j=1}^{N} \|\boldsymbol{r}_j - \boldsymbol{\tau}_j\| < \varepsilon$ if there exist parameters $\gamma_i, \alpha_i, \boldsymbol{\beta}_i$ such that the following conditions are satisfied

$$\boldsymbol{H}(\boldsymbol{x}, \boldsymbol{\gamma}, \boldsymbol{\alpha})\boldsymbol{\beta} \approx \boldsymbol{T} \tag{17}$$

where the output matrix of the hidden layer is given by (18).

$$\boldsymbol{H}(\boldsymbol{x}, \boldsymbol{\gamma}, \boldsymbol{\alpha}) = \begin{bmatrix} J(x_1, \gamma_1, \alpha_1) & \cdots & J(x_1, \gamma_{\widetilde{N}}, \alpha_{\widetilde{N}}) \\ \vdots & \cdots & \vdots \\ J(x_N, \gamma_1, \alpha_1) & \cdots & J(x_N, \gamma_{\widetilde{N}}, \alpha_{\widetilde{N}}) \end{bmatrix} \in \boldsymbol{R}^{N \times \widetilde{N}} \tag{18}$$

$$\boldsymbol{x} = [x_1\ x_2\ \cdots x_{\widetilde{N}}], \boldsymbol{\gamma} = [\gamma_1\ \gamma_2\ \cdots \gamma_{\widetilde{N}}]$$

$$\boldsymbol{\alpha} = [\alpha_1\ \alpha_2\ \cdots \alpha_{\widetilde{N}}]$$

$$\boldsymbol{\beta} = \left[\beta_1^T\ \beta_2^T\ \cdots \beta_{\widetilde{N}}^T\right]^T \epsilon \boldsymbol{R}^{\widetilde{N} \times m}, \text{ and}$$

$$\boldsymbol{T} = [\tau_1^T\ \tau_2^T\ \cdots \tau_{\mathrm{N}}^T]^T \epsilon \boldsymbol{R}^{N \times m}$$

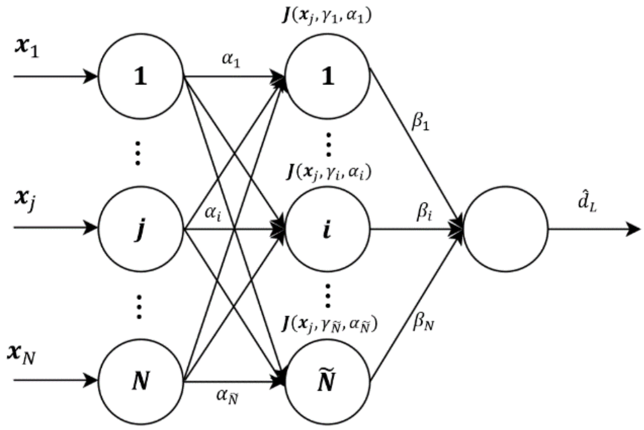

Fig. 3. The structure of the SLFN consisting of $\widetilde{N}$ hidden-layer nodes [79]

D. Proposed Method: Design of ELMRPDC

To proceed with the design of the proposed ELMRPDC, the error dynamics is established as the foundation for developing the control strategy. The block diagram of the ELMRPDC system is shown in Fig. 4. Based on the tracking error (10), the tracking error dynamics is derived as follows:

$$\ddot{e}(t) = \ddot{r}(t) - \ddot{x}(t) \tag{19}$$

Substituting (9) into (19), resulting in:

$$\ddot{e}(t) = \ddot{r}(t) - a_0\dot{x}(t) - b_0 u(t) - b_0 d_i(t) \tag{20}$$

As shown in Fig. 4, $e_R(t)$ is defined as $e_R(t) = e(t) + x_R(t)$. Therefore, $\ddot{e}_R(t)$ can be formulated as

$$\ddot{e}_R(t) = \ddot{r}(t) - a_0\dot{x}(t) - b_0 u(t) - b_0 d_i(t) + \ddot{x}_R(t) \tag{21}$$

Consider the lump disturbance $d_L(t)$ as $d_L(t) = b_0 d_i(t) - \ddot{x}_R(t)$, thus (21) becomes

$$\ddot{e}_R(t) = \ddot{r}(t) - a_0\dot{x}(t) - b_0 u(t) - d_L(t) \tag{22}$$

The sigmoid function is selected as the activation function for the neural network to estimate the disturbance $d_L(t)$, as defined (23).

$$J(x, \gamma, \alpha) = \frac{1}{1 + e^{-(\gamma \cdot x + \alpha)}} \tag{23}$$

where input weight γ and bias α are initially chosen at random. Sigmoidal activation functions are widely utilized in ELM due to its smooth differentiability, universal approximation capabilities, and ability to capture complex nonlinear interactions [80]. Sigmoidal functions are also useful for adaptive control in control systems because they offer steady learning dynamics and avoid sudden changes in network output. Furthermore, it helps guarantee bounded activation values, avoiding excessive weight updates that can cause the system to become unstable.

Let the actual disturbance be expressed as $d_L(t) = H\beta^*$, where β^* is the ideal network output weight matrix and H is the hidden layer output matrix. To design an RC with the inclusion of PD control, the control surface is introduced as follows:

$$\sigma_R(t) = (s + K_p)e_R(t) = \dot{e}_R(t) + K_p e_R(t) \tag{24}$$

where K_p is the proportional gain. In this case, derivative gain is set to 1.

Remark 1: The proportional gain K_p in (24) is chosen as a positive value to ensure that the controller zero is located in the left half-plane (LHP), resulting in a stable σ_R. This is crucial for maintaining system stability, as a zero in the LHP ensures that responses in the time domain is bounded given the bounded input.

Then, taking the first derivative of (24), we get

$$\dot{\sigma}_R(t) = \ddot{e}_R(t) + K_p \dot{e}_R(t) \tag{25}$$

Substituting (22) into (25), resulting in

$$\begin{aligned} \dot{\sigma}_R(t) = \ddot{r}(t) - a_0\dot{x}(t) - b_0 u(t) - d_L(t) \\ + K_p \dot{e}_R(t) \end{aligned} \tag{26}$$

Then, (26) can also be expressed as

$$\begin{aligned} \dot{\sigma}_R(t) = \ddot{r}(t) - a_0\dot{x}(t) - b_0 u(t) - \hat{d}_L(t) \\ + [\hat{d}_L(t) - d_L(t)] + K_p \dot{e}_R(t) \end{aligned} \tag{27}$$

Finally, the proposed control law $u(t)$ is defined as $u(t) = u_1(t) + u_2(t)$, where $u_1(t)$ and $u_2(t)$ are given by

$$\begin{aligned} u_1(t) = \frac{1}{b_0}\big[a_0\dot{x}(t) - b_0 u(t) - \ddot{r}(t) + K_p \dot{e}_R(t) \\ + K_\sigma \sigma_R(t)\big] \end{aligned} \tag{28}$$

$$u_2(t) = \frac{1}{b_0}[-\hat{d}_L(t)] \tag{29}$$

where K_σ represents a control surface gain, and $\hat{d}_L(t)$ is the estimated disturbance $d_L(t)$. The estimated disturbance $\hat{d}_L(t)$ is defined as $\hat{d}_L(t) = H\hat{\beta}$, where $\hat{\beta}$ is the estimate of the output weight matrix. The output weight matrix estimation $\hat{\beta}$ is updated with the adaptive law $\dot{\hat{\beta}}^T$ as (30)

$$\dot{\hat{\beta}}^T = -\eta \sigma_R(t) H \tag{30}$$

where η is the learning rate.

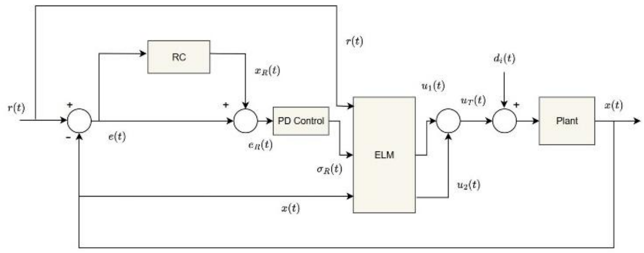

Fig. 4. Block diagram of ELMRPDC

Remark 2: The selection of gains and variables in the control law $u(t)$, including the learning rate η, the number of hidden layer neurons, the proportional gain K_p, the control surface gain K_σ, generally follows a rule-of-thumb approach based on common practical ranges. These parameters are typically chosen through empirical tuning or prior studies to balance stability, convergence speed, and overall control performance. Proper selection ensures effective adaptation and robustness of the system while preventing issues such as overfitting, instability, or slow response.

E. Stability Analysis

The stability analysis in this study is conducted using Lyapunov approach. The Lyapunov candicate function is firstly chosen based on the control surface $\sigma_R(t)$ and the estimation error $\tilde{\beta}$, which represent the system errors. The Lyapunov function is defined as

$$V = \frac{1}{2}{\sigma_R}^2(t) + \frac{1}{\eta}\tilde{\beta}^T\tilde{\beta} \tag{31}$$

The first derivative of (31) is

$$\dot{V} = \sigma_R(t)\dot{\sigma}_R(t) + \frac{1}{\eta}\dot{\tilde{\beta}}^T\tilde{\beta} \tag{32}$$

It follows that we need to obtain the dynamics of $\dot{\sigma}_R(t)$ by substituting the control law $u(t) = u_1(t) + u_2(t)$ into (27). Then, we get

$$\begin{aligned} \dot{\sigma}_R(t) = \ddot{r}(t) - a_0\dot{x}(t) - b_0[u_1(t) + u_2(t)] \\ - \hat{d}_L(t) + \big[\hat{d}_L(t) - d_L(t)\big] \\ + K_p \dot{e}_R(t) \end{aligned} \tag{33}$$

$$\begin{aligned} \dot{\sigma}_R(t) = \ddot{r}(t) - a_0\dot{x}(t) - b_0 u_1(t) - b_0 u_2(t) \\ - \hat{d}_L(t) + \big[\hat{d}_L(t) - d_L(t)\big] \\ + K_p \dot{e}_R(t) \end{aligned}$$

Substituting (28) and (29) into (33), resulting in (34).

$$\dot{\sigma}_R = \ddot{r}(t) - a_0\dot{x}(t) - b_0\left[\frac{1}{b_0}\left(a_0\dot{x}(t) - b_0u(t) - \ddot{r}(t) + K_p\dot{e}_R(t) + K_\sigma\sigma_R(t)\right) + \frac{1}{b_0}(-\hat{d}_L(t))\right] - \hat{d}_L(t) + [\hat{d}_L(t) - d_L(t)] + K_p\dot{e}_R(t) \tag{34}$$

$$\dot{\sigma}_R = \ddot{r}(t) - a_0\dot{x}(t) + a_0\dot{x}(t) - \ddot{r}(t) - K_p\dot{e}_R(t) - K_\sigma\sigma_R(t) + \hat{d}_L(t) - \hat{d}_L(t) + \hat{d}_L(t) - d_L(t) + K_p\dot{e}_R(t)$$

Simplifying (34), we have

$$\dot{\sigma}_R = -K_\sigma\sigma_R(t) + \hat{d}_L(t) - d_L(t) \tag{35}$$

Consider that

$$d_L(t) - \hat{d}_L(t) = H\beta^* - H\hat{\beta} = H\left[\beta^* - \hat{\beta}\right] = H\tilde{\beta} \tag{36}$$

Based on (36), (35) can be expressed as

$$\dot{\sigma}_R = -K_\sigma\sigma_R(t) - H\tilde{\beta} \tag{37}$$

With the adaptive law (30), $\dot{\tilde{\beta}}^T$ in (32) can be derived as follows:

$$\dot{\tilde{\beta}}^T = \dot{\beta}^{*T} - \dot{\hat{\beta}}^T = 0 - \dot{\hat{\beta}}^T = \eta\sigma_R(t)H \tag{38}$$

Substituting (37) and (38) into (32), then

$$\begin{aligned} \dot{V} &= \sigma_R(t)[-K_\sigma\sigma_R(t) - H\tilde{\beta}] + \frac{1}{\eta}[\eta\sigma_R(t)H]\tilde{\beta} \\ &= -K_\sigma{\sigma_R}^2(t) - \sigma_R(t)H\tilde{\beta} + \frac{1}{\eta}[\eta\sigma_R(t)H]\tilde{\beta} \\ &= -K_\sigma{\sigma_R}^2(t) - \sigma_R(t)H\tilde{\beta} + \sigma_R(t)H\tilde{\beta} \\ &= -K_\sigma{\sigma_R}^2(t) \end{aligned} \tag{39}$$

Remark 3: From (39), it can be seen that the derivative of the Lyapunov function $\dot{V}$, is negative definite, satisfying the stability condition $\dot{V} < 0$, provided that K_σ is chosen as a positive gain. With K_σ selected as a positive gain, the system is guaranteed to be stable, and the convergences of the control surface $\sigma_R(t)$ and the estimation error $\tilde{\beta}(t)$ are ensured. This also implies the guaranteed convergences of the RC error $e_R(t)$ and the tracking error $e(t)$.

F. Robustness Analysis

In practical implementations, system parameters such as K and τ may vary due to modeling inaccuracies, component aging, or environmental factors. These variations affect the system dynamics by introducing uncertainties in the coefficients a_0 and b_0, leading to deviations Δa_0 and Δb_0. Consequently, the lumped disturbance $d_L(t)$ differs from the nominal case, impacting system model. The perturbed system can be expressed as:

$$\ddot{x}(t) = (a_0 + \Delta a_0)\dot{x}(t) + (b_0 + \Delta b_0)[u(t) + d_i(t)] \tag{40}$$

$$\ddot{x}(t) = a_0\dot{x}(t) + b_0u(t) + (b_0 + \Delta b_0)d_i(t) + \Delta a_0\dot{x}(t) + \Delta b_0u(t)$$

where the lumped disturbance estimate $\hat{d}_L(t)$ is given by:

$$\hat{d}_L(t) = b_0d_i(t) + \Delta b_0d_i(t) + \Delta a_0\dot{x}(t) + \Delta b_0u(t) \tag{41}$$

To compensate for these uncertainties, the adaptive law in (30) adjusts $\hat{\beta}$ to estimate the lumped disturbance $\hat{d}_L(t)$ (41) instead of the input disturbance $b_0d_i(t)$ only as in the nominal case. Therefore, this new disturbance estimation and compensation will ensure robustness against system model variations and input disturbances. This adaptive mechanism enhances the system's ability to maintain tracking accuracy despite parameter changes and unmodeled disturbances.

This additional robustness analysis reinforces the effectiveness of the ELMRPDC framework, demonstrating its capability to handle real-world uncertainties beyond the modeled disturbances, thereby improving its reliability in dynamic environments. To ensure a comprehensive evaluation of the proposed ELMRPDC method, we first analyze its robustness against various disturbances and its ability to maintain stability. Building on these insights, the next step is to outline the methodology used in this study.

In this study, we focus on evaluating the performance of the proposed ELMRPDC method in terms of tracking accuracy, robustness against different types of disturbances, and overall system stability. The methodology involves integrating ELM and RPDC to form ELMRPDC, followed by stability verification using the Lyapunov theorem. The control strategy is then applied to a servomotor model, subjected to various disturbances, including sinusoidal, time-varying sinusoidal, multi-period sinusoidal, and aperiodic disturbances. The systems performance is assessed using RMSE and MAE metrics, followed by further analysis. A summary of the research methodology is illustrated in the flowchart shown in Fig. 5.

III. RESULTS AND DISCUSSION

In this simulation, the continuous-time model of the Quanser SRV02 servo [81], as described in (9) is used and expressed as follows:

$$\ddot{x} = a_0\dot{x}(t) + b_0u(t) + b_0d_i(t), \tag{42}$$

where $a_0 = -37.3134$, and $b_0 = 64.9253$. The reference signal $r(t)$ used in this simulation is depicted in Fig. 6, and modeled as (43).

$$r(t) = \sin(\pi t) \tag{43}$$

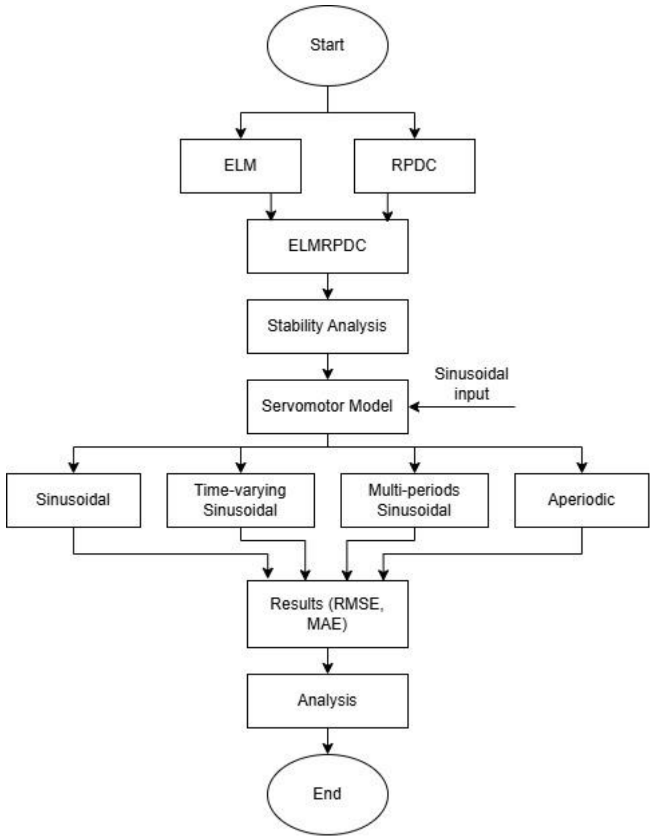

Fig. 5. Flowchart of research methodology

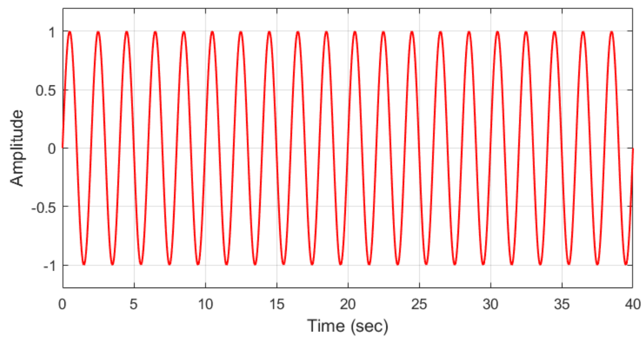

Fig. 6. Reference signal $r(t)$

In addition to reference tracking, the plant is subjected to four types of disturbances: sinusoidal, time-varying, multi-periodic, and aperiodic. The disturbance models are listed in Table I and illustrated in Fig. 7 to Fig. 10. These disturbances are introduced to assess the robustness of both ELMRPDC and RPDC under challenging conditions.

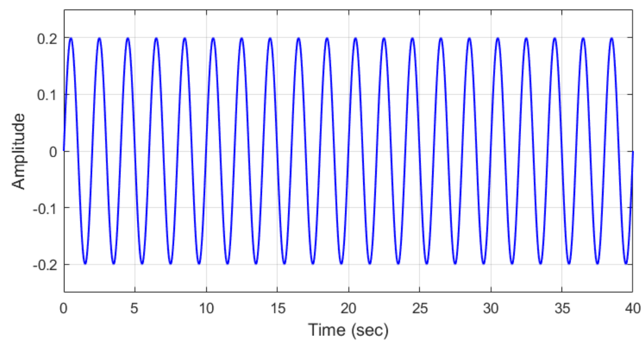

Fig. 7. Sinusoidal disturbance $d_1(t)$

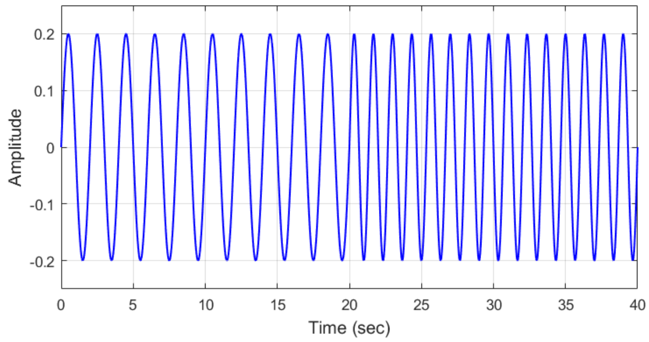

Fig. 8. Time-varying sinusoidal disturbance $d_2(t)$

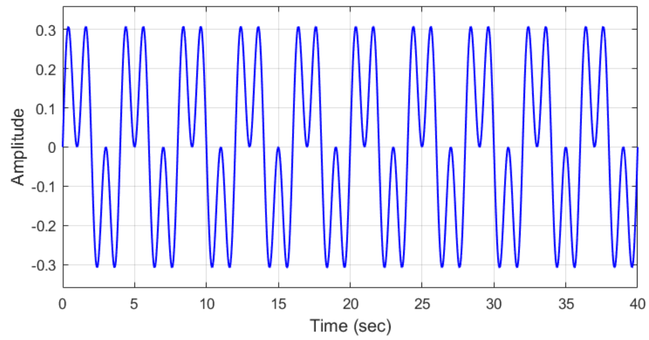

Fig. 9. Multi-periods sinusoidal disturbance $d_3(t)$

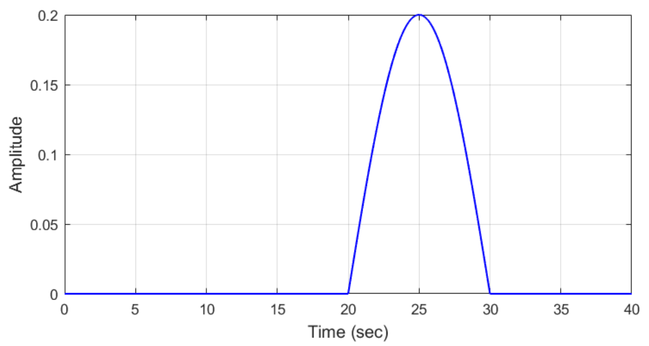

Fig. 10. Aperiodic disturbance $d_4(t)$

TABLE I. DISTURBANCE MODELS

Dist.	Type	Value
$d_1(t)$	Sinusoidal	$d_1(t) = 0.2\sin(\pi t)$
$d_2(t)$	Time-varying sinusoidal	$d_2(t) = \begin{cases} 0.2\sin(\pi t), 0 \le t \le 20 \\ 0.2\sin(1.5\pi t), 20 \le t \le 40 \end{cases}$
$d_3(t)$	Multi-periods sinusoidal	$d_3(t) = 0.2\sin(0.5\pi t) + 0.2\sin(1.5\pi t)$
$d_4(t)$	Aperiodic	See Fig. 10

In this simulation, the RC is formulated as follows.

$$\frac{X_R(s)}{E(s)} = \frac{\dfrac{\omega_c}{s+\omega_c} e^{-sT_R}}{1 - \dfrac{\omega_c}{s+\omega_c} e^{-sT_R}}, \tag{44}$$

where the delay length $T_R = 2\ s$ and $\omega_c = 2\pi f_c$ with frequency cut-off $f_c = 5\ Hz$. Here, the delay length T_R is determined based on the reference model (43). The proportional gain K_p and the control surface gain K_σ are set to 2.4 and 1.2, respectively. For the ELM, a learning rate η of 0.5 is selected based on a rule-of-thumb approach, as discussed in the remark, and further validated through trial and error to achieve a balance between convergence speed and stability. The initial input weight γ and input bias α are randomly initialized within the intervals [-1,1] and [0,1], respectively. The input weights in ELM are randomly selected within [-1,1] to ensure diverse feature mapping, while input biases are chosen from [0,1] to maintain stability in activation. This randomization supports ELM's universal approximation property, allowing it to efficiently learn without iterative tuning. Additionally, it improves generalization and computational efficiency by eliminating the need for gradient-based optimization [80]. The number of neurons in the hidden layer was varied from 100 to 2000, with an increment of 100 neurons for each variation.

MATLAB/Simulink is used to simulate the performance of ELMRPDC and RPDC for simultaneous tracking and disturbance rejection. For analysis, metrics such as root-mean-square error (RMSE) and maximum absolute error (MAE) are used, as defined below.

$$RMSE = \sqrt{\frac{1}{Ns}\sum_{i=1}^{Ns}(e^2(t))} \tag{45}$$

$$MAE = \frac{1}{Ns}\sum_{i=1}^{Ns}|e(t)| \tag{46}$$

where Ns represents the number of samples collected over the timeframe of 0–40 seconds.

A. Tracking Performance with Sinusoidal Disturbance $d_1(t)$

The present study demonstrates that the ELMRPDC method significantly improves tracking performance in systems subjected to sinusoidal disturbances $d_1(t)$ compared to the conventional RPDC approach. For the case of a sinusoidal disturbance, ELMRPDC achieves its optimal performance with a hidden layer size of 800 neurons, resulting in an RMSE of 1.6681 degrees and an MAE of 10.4101 degrees based on Table II. This represents a substantial improvement over RPDC, which yields an RMSE of 2.9636 degrees and an MAE of 19.1064 degrees. The absolute error $|e(t)|$ comparison, as shown in Fig. 11, further confirms that ELMRPDC consistently maintains lower error levels throughout the simulation, particularly after the transient phase.

The superior performance of ELMRPDC can be attributed to the adaptive capabilities of the ELM, which effectively estimates and compensates for sinusoidal disturbances. The improvement in tracking accuracy, as evidenced by the reduction in RMSE and MAE by 43.7137% and 45.5146%, respectively, underscores the importance of integrating ELM into repetitive control frameworks. This finding suggests that ELMRPDC is particularly well-suited for applications requiring precise tracking in the presence of periodic disturbances. Additionally, the study highlights the critical role of selecting an appropriate hidden layer size, as smaller networks (e.g., 100 neurons) may underperform compared to RPDC, while larger networks (e.g., 800 neurons) achieve optimal results.

TABLE II. THE TRACKING PERFORMANCE OF ELMRPDC WITH SINUSOIDAL DISTURBANCE

#Hidden-layer Neurons	RMSE (deg)	MAE (deg)
100	7.5783	30.1757
200	3.9726	20.6254
300	2.6541	15.5178
400	2.0866	12.6000
500	1.8286	11.2356
600	1.7197	10.6050
700	1.6738	10.4732
800	1.6681	10.4101
900	1.6738	10.4388
1000	1.6853	10.5993
1100	1.6968	10.6853
1200	1.7140	10.8114
1300	1.7312	10.8343
1400	1.7484	10.9719
1500	1.7598	11.0751
1600	1.7770	11.1898
1700	1.7885	11.3847
1800	1.8000	11.3216
1900	1.8114	11.4477
2000	1.8229	11.4878

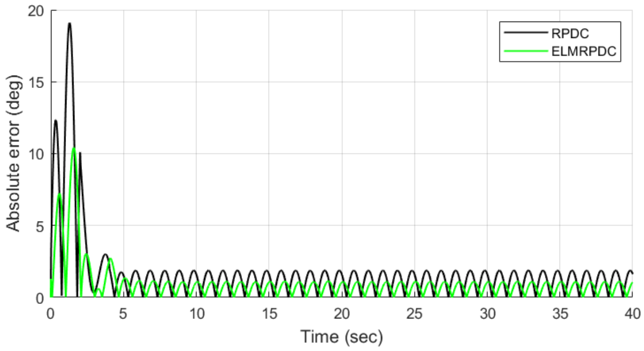

Fig. 11. Absolute errors $|e(t)|$ for RPDC and ELMRPDC (with 800 hidden-layer neurons) under sinusoidal disturbance

B. Tracking Performance with Time-Varying Sinusoidal Disturbance $d_2(t)$

The study evaluates the performance of ELMRPDC in handling a time-varying disturbance $d_2(t)$, involves a sudden change in the disturbance frequency from 0.5 Hz to 0.75 Hz at $t = 20\,s$, posing a challenging disturbance rejection scenario. This scenario presents a more challenging control problem compared to a fixed-frequency disturbance. Based on Table III, the results show that ELMRPDC achieves its optimal performance with 900 hidden-layer neurons, yielding an RMSE of 1.7369 degrees and an MAE of 10.4388 degrees. In contrast, the conventional RPDC method produces significantly higher errors, with an RMSE of 3.2044 degrees and an MAE of 19.1064 degrees. This shows that ELMRPDC can adjust to abrupt modifications in the frequency of disturbances while keeping error levels low during the simulation. As illustrated in Fig. 12, the absolute error $|e(t)|$ comparison provides additional support.

The superior performance of ELMRPDC in this case can be attributed to the adaptive nature of the ELM, which dynamically adjusts to changes in disturbance frequency. The reduction in RMSE and MAE by 45.7960% and 45.3645%, respectively, compared to RPDC, underscores the effectiveness of ELMRPDC in handling time-varying disturbances. This improvement is particularly evident after the frequency transition at $t = 20\,s$, where ELMRPDC quickly stabilizes the system, while RPDC experiences significant error spikes. These findings suggest that ELMRPDC is highly effective for applications where disturbances exhibit frequency variations, such as in industrial automation or robotics.

TABLE III. THE TRACKING PERFORMANCE OF ELMRPDC WITH TIME-VARYING SINUSOIDAL DISTURBANCE

#Hidden-layer Neurons	RMSE (deg)	MAE (deg)
100	7.4980	30.1757
200	4.0815	20.6254
300	2.8146	15.5006
400	2.2471	12.5942
500	1.9719	11.2299
600	1.8401	10.6050
700	1.7770	10.4732
800	1.7484	10.4101
900	1.7369	10.4388
1000	1.7426	10.5993
1100	1.7484	10.6853
1200	1.7598	10.8114
1300	1.8802	10.2439
1400	1.8687	10.4445
1500	1.7885	11.0751
1600	1.8000	11.1898
1700	1.8114	11.2815
1800	1.8171	11.3216
1900	1.8280	11.4477
2000	1.8401	11.4878

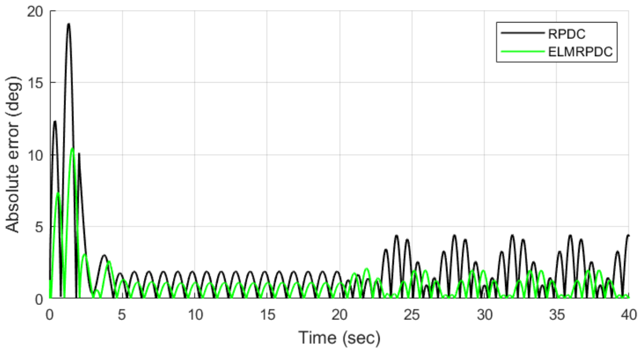

Fig. 12. Absolute errors $|e(t)|$ for RPDC and ELMRPDC (with 900 hidden-layer neurons) under time-varying sinusoidal disturbance

C. *Tracking Performance with Multi-Periods Sinusoidal Disturbance* $d_3(t)$

This study investigates the performance of ELMRPDC in handling a multi-periodic disturbance $d_3(t)$, which consists of two frequency components: 0.25 Hz and 0.75 Hz. This scenario presents a highly challenging control problem due to the simultaneous presence of multiple disturbance frequencies. The results reveal that ELMRPDC achieves its optimal performance with 1500 hidden-layer neurons, yielding an RMSE of 1.8630 degrees and an MAE of 10.6050 degrees based on Table IV. In contrast, the conventional RPDC method produces significantly higher errors, with an RMSE of 5.7267 degrees and an MAE of 20.7287 degrees. This demonstrates that ELMRPDC is capable of effectively compensating for multi-periodic disturbances, maintaining superior tracking accuracy throughout the simulation.

The superior performance of ELMRPDC in this case can be attributed to the ELM's ability to simultaneously estimate and compensate for multiple disturbance frequencies. The reduction in RMSE and MAE by 67.4674% and 57.9093%, respectively, compared to RPDC, highlights the effectiveness of ELMRPDC in handling multi-periodic disturbances. This improvement is particularly evident in the absolute error plot in Fig. 13, where ELMRPDC maintains consistently lower error levels compared to RPDC, even in the presence of complex disturbance dynamics. These findings suggest that ELMRPDC is highly effective for applications where disturbances consist of multiple frequency components, such as in precision manufacturing or advanced robotics.

TABLE IV. THE TRACKING PERFORMANCE OF ELMRPDC WITH MULTI-PERIODS SINUSOIDAL DISTURBANCE

#Hidden-layer Neurons	RMSE (deg)	MAE (deg)
100	10.9031	30.9439
200	6.5464	17.2490
300	4.4713	13.0356
400	3.4280	10.0433
500	2.8203	8.9484
600	2.4707	8.7248
700	2.2471	8.9484
800	2.1038	9.1719
900	2.0178	9.4012
1000	1.9547	9.7280
1100	1.9203	9.9343
1200	1.8917	10.1522
1300	1.8802	10.2496
1400	1.8687	10.4445
1500	1.8630	10.6050
1600	1.8630	10.7598
1700	1.8630	10.8917
1800	1.8630	10.9547
1900	1.8630	11.1095
2000	1.8687	11.1668

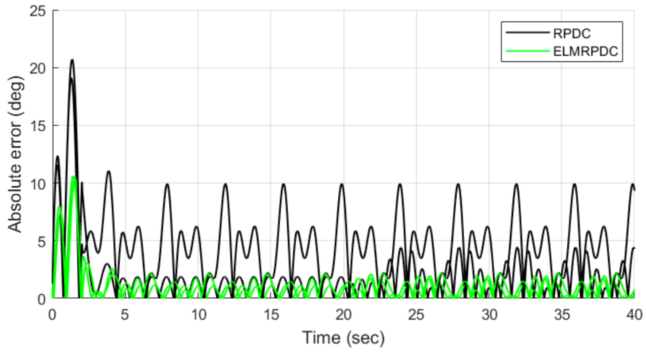

Fig. 13. Absolute errors $|e(t)|$ for RPDC and ELMRPDC (with 1500 hidden-layer neurons) under multi-periods sinusoidal disturbance

D. *Tracking Performance with Aperiodic Disturbance* $d_4(t)$

This study examines the performance of ELMRPDC in handling an aperiodic disturbance $d_4(t)$, which lacks a repetitive pattern and appears only during the time interval $t = 20 - 30\,s$. This scenario presents a unique challenge for control systems, as aperiodic disturbances are inherently unpredictable. Based on Table V, the results show that ELMRPDC achieves its optimal performance with 700 hidden-layer neurons, yielding an RMSE of 1.5133 degrees and an MAE of 9.4127 degrees. In contrast, the conventional RPDC method produces higher errors, with an RMSE of 3.0439 degrees and an MAE of 18.4529 degrees. This demonstrates that ELMRPDC is capable of effectively compensating for aperiodic disturbances, provided the hidden-layer size is appropriately configured.

The superior performance of ELMRPDC in this case can be attributed to the ELM's ability to adaptively estimate and compensate for non-repetitive disturbances. The reduction in RMSE and MAE by 50.2824% and 49.2078%, respectively, compared to RPDC, underscores the effectiveness of ELMRPDC in handling aperiodic disturbances. This improvement is particularly evident during the disturbance interval $t = 20 - 30\ s$, where ELMRPDC maintains lower error levels compared to RPDC, as shown in Fig. 14. These findings suggest that ELMRPDC is highly effective for applications where disturbances are irregular or unpredictable, such as in aerospace systems or advanced robotics.

TABLE V. THE TRACKING PERFORMANCE OF ELMRPDC WITH APERIODIC DISTURBANCE

#Hidden-layer Neurons	RMSE (deg)	MAE (deg)
100	7.2859	29.5280
200	3.6802	18.2579
300	2.3732	13.7751
400	1.8286	10.9949
500	1.6050	9.8082
600	1.5248	9.3726
700	1.5133	9.4127
800	1.5248	9.4987
900	1.5477	9.6420
1000	1.5764	9.9000
1100	1.5993	10.0605
1200	1.6280	10.2439
1300	1.6509	10.3184
1400	1.6738	10.5019
1500	1.6968	10.6452
1600	1.7140	10.7885
1700	1.7312	10.9089
1800	1.7484	10.9777
1900	1.7656	11.1210
2000	1.7770	11.1840

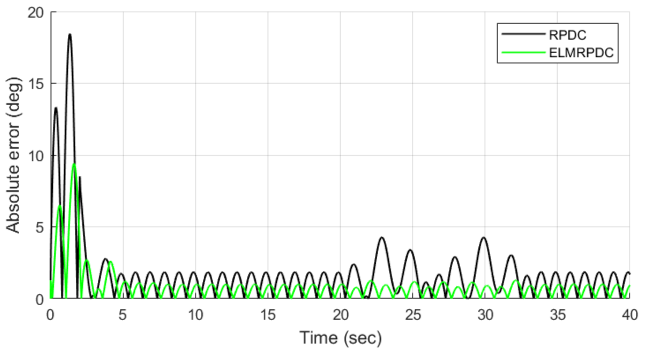

Fig. 14. Absolute errors $|e(t)|$ for RPDC and ELMRPDC (with 700 hidden-layer neurons) under aperiodic disturbance

Finally, the comparative performance of RPDC and optimal ELMRPDC in terms of RMSE and MAE is presented in Table VI, providing a clear evaluation of their tracking accuracy and disturbance compensation capabilities.

TABLE VI. COMPARISON OF RMSE AND MAE FOR RPDC AND OPTIMAL ELMRPDC UNDER VARIOUS DISTURBANCES

Dist.	ELMRPDC		RPDC	
	RMSE (deg)	MAE (deg)	RMSE (deg)	MAE (deg)
d_1	1.6681 (at 800-neuron)	10.4101 (at 800-neuron)	2.9636	19.1064
d_2	1.7369 (at 900-neuron)	10.4388 (at 900-neuron)	3.2044	19.1064
d_3	1.8630 (at 1500-neuron)	10.6050 (at 1500-neuron)	5.7267	20.7287
d_4	1.5133 (at 700-neuron)	9.4127 (at 700-neuron)	3.0439	18.4529

Table VI demonstrates that ELMRPDC consistently outperforms RPDC in both RMSE and MAE across all four disturbance types, provided the hidden-layer neuron size is appropriately tuned. This highlights the benefit of integrating ELM into the RPDC architecture to enhance tracking performance under challenging disturbance conditions. ELMRPDC demonstrates superior disturbance rejection by utilizing ELM's capability to adapt to the dynamic disturbances. It demonstrates greater resilience and flexibility than standalone RPDC, particularly in managing uncertain or varying disturbance. The findings of this study demonstrate that integrating ELM into RPDC significantly enhances tracking accuracy and disturbance rejection capabilities compared to conventional RPDC. This study also provides new insights into the impact of the number of hidden-layer neurons on ELMRPDC performance across various disturbance scenarios, including sinusoidal, time-varying, multi-periodic, and aperiodic disturbances.

The results confirm that increasing the number of neurons improves system performance, though the optimal number varies depending on the complexity of the disturbance. For fixed-frequency disturbances, a moderately sized hidden layer (800 neurons) is sufficient, whereas more complex disturbances, such as multi-periodic ones, require larger networks (up to 1500 neurons). In the case of aperiodic disturbances, which lack repetitive patterns, a more moderate hidden-layer size (700 neurons) still provides significant improvements. While performance improves with an increase in hidden layer size, ELMRPDC follows a distinct pattern, indicating the existence of an optimal range beyond which further addition of neurons yields only marginal improvements.

Extensive simulations were conducted to determine the optimal number of hidden layer neurons in ELM, as this parameter significantly influences system performance. The results revealed that, across all tested scenarios, the optimal range of hidden layer neurons remained relatively consistent. This finding suggests that a general guideline for selecting the number of neurons can be established, reducing the need for exhaustive tuning in future implementations. The findings of this study have significant practical implications, particularly in real-world applications where computational efficiency and adaptability are crucial. With advancements in processor capabilities, the implementation of ELMRPDC in real-time control systems is feasible, as ELM requires relatively low computational resources compared to multi-hidden layer neural networks and deep learning models.

The computational cost associated with increasing the number of hidden-layer neurons in ELM is acknowledged as a trade-off in achieving optimal performance. However, ELM has been shown to be significantly faster compared to traditional learning algorithms. As demonstrated in [80], ELM runs approximately 300 times faster than the BP algorithm and 15 times faster than SVM, even for relatively complex tasks. Moreover, while theoretically, ELM can approximate any continuous function with sufficient hidden-layer neurons [82], the selection of the optimal number of neurons remains a crucial aspect to balance accuracy and efficiency. Arbitrarily increasing hidden neurons may lead to underfitting or overfitting, and thus, strategies such as incremental constructive methods have been suggested to optimize the hidden-layer structure dynamically [83]. In this study, the number of hidden neurons was determined through trial and error, which is a common practice in ELM-based implementations [84]. Although a larger number of neurons may increase matrix computational complexity [85], modern processors can handle such computations efficiently, and the lightweight nature of ELM compared to multi-hidden-layer neural networks ensures that real-time feasibility remains viable.

To further highlight the effectiveness of ELMRPDC, it is possible to compare it with conventional control strategies, such as proportional-derivative repetitive control (PD-RC) in [86], which has been widely used for disturbance rejection. Despite its advantages, this method faces several challenges that limit its real-world applicability. PD-RC relies on precise system models to compensate for disturbances effectively. However, friction characteristics in real-world systems are often unknown and time-varying, making model-based controllers highly susceptible to significant modeling errors. In contrast, ELMRPDC leverages data-driven learning through ELM, which does not require an accurate model, making it more adaptable to system uncertainties. ELMRPDC mitigates issues related to nonlinear frictional effects by learning and compensating for them, reducing limit cycles and improving steady-state performance.

Because of this, the ELMRPDC approach is a good option for real-time, high-speed applications that require quick adaptability and rejection of disturbances. Future research could explore adaptive methods to optimize hidden-layer neuron selection dynamically, reducing the computational burden while maintaining robust performance. Additionally, the approach can be extended to multivariable systems and applied in areas like industrial automation, robotics, and vibration compensation in machinery, where precise tracking and disturbance rejection are crucial.

IV. CONCLUSION

This study introduces ELMRPDC, a hybrid control strategy that integrates RPDC with ELM to enhance reference tracking and disturbance rejection. By leveraging ELM, the proposed method effectively overcomes a key limitation of RC—its inability to compensate for time-varying periodic, multi-periodic, and aperiodic disturbances. The inclusion of ELM enables real-time adaptation and compensation, significantly improving system robustness against various types of disturbances. Simulation results demonstrated the superior performance of ELMRPDC compared to standalone RPDC, particularly in its ability to track periodic reference signals and reject disturbances. Additionally, the study highlighted the critical influence of the number of hidden layer neurons in ELM, where variations in neuron count significantly impacted system performance. This underscores the importance of optimizing this parameter to achieve the best control outcomes. Despite its advantages, the proposed method presents certain challenges. Determining the optimal number of hidden layer neurons requires extensive simulations, which can be considered a drawback. However, with modern processors, the computational burden is not a significant issue. ELM, being a lightweight machine learning algorithm, is computationally more efficient than multi-hidden-layer neural networks and deep learning approaches, making real-time implementation feasible. Future research should focus on extending this approach to multivariable systems and conducting experimental validation on real-world scenarios. One promising application is in machinery requiring vibration compensation, where precise disturbance rejection and adaptability are crucial for maintaining stability and performance.

ACKNOWLEDGMENT

The authors would like to thank the National Research and Innovation Agency (BRIN) for funding research through Degree by Research (DBR) and Research Assistant (RA) programs. This research was also supported by the Research Center for Photonics and the Deputy for Research and Innovation Infrastructure (DIRI) under the National Research and Innovation Agency (BRIN), Indonesia.

REFERENCES

[1] T. Inoue, M. Nakano, T. Kubo, S. Matsumoto, and H. Baba, “High Accuracy Control of a Proton Synchrotron Magnet Power Supply,” *IFAC Proc. Vol.*, vol. 14, no. 2, pp. 3137–3142, 1981, doi: 10.1016/S1474-6670(17)63938-7.

[2] B. A. Francis and W. M. Wonham, “The internal model principle for linear multivariable regulators,” *Appl. Math. Optim.*, vol. 2, no. 2, pp. 170–194, 1975, doi: 10.1007/BF01447855.

[3] R. L. McGrath and F. Sergi, “Repetitive Control of Knee Interaction Torque via a Lower Extremity Exoskeleton for Improved Transparency During Walking,” *IEEE Trans. Med. Robot. Bionics*, vol. 6, no. 4, pp. 1581–1590, 2024, doi: 10.1109/TMRB.2024.3464119.

[4] K. Umeda, Y. Jiang, H. Yokoi, and S. Togo, "Repetitive Control of Robotic Joint With Variable Impedance Utilizing Agonist-Antagonist Muscle Pair Structure Based on Virtual Trajectories," in *IEEE Access*, vol. 13, pp. 16866-16878, 2025, doi: 10.1109/ACCESS.2025.3532633.

[5] L. Li, X. Wang, W.-W. Huang, X. Zhang, and L. Zhu, “Design of General Parametric Repetitive Control Using IIR Filter With Application to Piezo-Actuated Nanopositioning Stages,” *IEEE Trans. Autom. Sci. Eng.*, vol. 21, no. 2, pp. 2102–2112, 2024, doi: 10.1109/TASE.2023.3260340.

[6] L. Li, W.-W. Huang, X. Wang, and L. Zhu, “Dual-Notch-Based Repetitive Control for Tracking Lissajous Scan Trajectories With Piezo-Actuated Nanoscanners,” *IEEE Trans. Instrum. Meas.*, vol. 71, pp. 1–12, 2022, doi: 10.1109/TIM.2022.3169561.

[7] L. Zhou, D. Gao, J. She, X.-M. Zhang, and H. Yan, “Adaptive Spatial Repetitive-Control for Time-Varying Periodic Signals in a Rotational System,” *IEEE Trans. Automat. Contr.*, vol. 69, no. 6, pp. 4134–4141, 2024, doi: 10.1109/TAC.2023.3349316.

[8] S. Tian *et al.*, “Two-Dimensional Repetitive Control of Uncertain Takagi–Sugeno Systems Based on a New Equivalent-Input-Disturbance Estimator,” *IEEE Trans. Fuzzy Syst.*, vol. 32, no. 4, pp. 2366–2377, 2024, doi: 10.1109/TFUZZ.2024.3350744.

[9] E. Kurniawan, H. Wang, J. A. Prakosa, P. Purwowibowo, and E. B. Pratiwi, "An improved repetitive controller with fractional time-delay for discrete-time linear systems: Synthesis and comparison study," *ISA Trans.*, vol. 146, pp. 511–527, 2024, doi: 10.1016/j.isatra.2023.12.035.

[10] E. Kurniawan *et al.*, "Design of Fractional Order Odd-Harmonics Repetitive Controller for Discrete-Time Linear Systems with Experimental Validations," *Sensors*, vol. 22, no. 22, 2022, doi: 10.3390/s22228873.

[11] E. Kurniawan *et al.*, "Discrete-Time Design of Fractional Delay-Based Repetitive Controller with Sliding Mode Approach for Uncertain Linear Systems with Multiple Periodic Signals," *Fractal and Fractional*, vol. 9, no. 1, 2025, doi: 10.3390/fractalfract9010041.

[12] E. Kurniawan *et al.*, "Robust adaptive repetitive control for unknown linear systems with odd-harmonic periodic disturbances," *Sci. China Inf. Sci.*, vol. 65, no. 12, p. 222202, 2022, doi: 10.1007/s11432-022-3561-2.

[13] X. Ye, X. Tang, K. Xing, H. Wang, J. Yao, and T. Zhang, "Repetitive Control for Vibration Suppression of Bearingless Induction Motor," *IEEE Access*, vol. 12, pp. 60532–60540, 2024, doi: 10.1109/ACCESS.2024.3391292.

[14] L.-W. Shih and C.-W. Chen, "Model-free repetitive control design and implementation for dynamical galvanometer-based raster scanning," *Control Eng. Pract.*, vol. 122, p. 105124, 2022, doi: 10.1016/j.conengprac.2022.105124.

[15] P. Cui, H. Xu, Z. Liu, J. Li, and B. Han, "Improved Second-Order Repetitive Control With Parameter Optimization for Magnetically Suspended Rotor System," *IEEE Sens. J.*, vol. 20, no. 5, pp. 2294–2303, 2020, doi: 10.1109/JSEN.2019.2951764.

[16] Y. Zhao, C. Xie, C. Peng, and J. Zou, "Passivity-Based Design of Frequency Adaptive Repetitive Controller for LCL-Type Grid-Connected Inverters," *IEEE Trans. Power Electron.*, vol. 39, no. 4, pp. 4017–4028, 2024, doi: 10.1109/TPEL.2023.3347723.

[17] Q. Qian *et al.*, "Coordinated Self-Tuning Implementation of Repetitive Control and Active Damping for 400 Hz Inverter against Filter Inductance Fluctuation," *IEEE Trans. Power Electron.*, vol. 39, no. 12, pp. 15520–15535, 2024, doi: 10.1109/TPEL.2024.3446833.

[18] W. Xiong, Z. Wang, J. Na, B. Zhang, and S. Li, "Robust Predictive Disturbance Observer-Based Repetitive Control for Time-Delay Systems With Application to CVCF Inverters," *IEEE Trans. Ind. Electron.*, vol. 72, no. 2, pp. 1904–1913, 2025, doi: 10.1109/TIE.2024.3417982.

[19] J. Zhang, Z. Sun, Q. Zhao, and H. Li, "Frequency Adaptive Proportional Feedforward Repetitive Control Based on Farrow Structure Filter for LCL Grid-Tied Inverters," in *IEEE Access*, vol. 12, pp. 191120-191128, 2024, doi: 10.1109/ACCESS.2024.3510881.

[20] M. Zhu, Y. Ye, Y. Xiong, and Q. Zhao, "Multibandwidth Repetitive Control Resisting Frequency Variation in Grid-Tied Inverters," *IEEE J. Emerg. Sel. Top. Power Electron.*, vol. 10, no. 1, pp. 446–454, 2022, doi: 10.1109/JESTPE.2021.3077618.

[21] Q. Chen, Y. Li, Y. Hong, and H. Shi, "Prescribed-Time Robust Repetitive Learning Control for PMSM Servo Systems," *IEEE Trans. Ind. Electron.*, vol. 71, no. 11, pp. 14753–14763, 2024, doi: 10.1109/TIE.2024.3363757.

[22] B. Chen, Z. Huang, P. Sun, and G. Wei, "Harmonic Suppression for PMSM Applied to MSTMP Based on Virtual Even-Order Fractional Repetitive Controller," *IEEE Trans. Ind. Informatics*, vol. 20, no. 4, pp. 6289–6299, 2024, doi: 10.1109/TII.2023.3345465.

[23] Y.-H. Lan, J.-L. He, P. Li, and J.-H. She, "Optimal preview repetitive control with application to permanent magnet synchronous motor drive system," *J. Franklin Inst.*, vol. 357, no. 15, pp. 10194–10210, 2020, doi: 10.1016/j.jfranklin.2020.04.026.

[24] S. Chalia, A. K. Seth, and M. Singh, "Frequency Adaptive Discrete Repetitive Controller Design for Electric Vehicle Charger," *IEEE J. Emerg. Sel. Top. Ind. Electron.*, vol. 6, no. 1, pp. 72–81, 2025, doi: 10.1109/JESTIE.2024.3469569.

[25] N. Feng, Y. Ruan, and T. Tang, "Youla Parameterization-Based Fractional Repetitive Control of Arbitrary Frequency Disturbance Rejections for Line-of-Sight Stabilization," *IEEE Trans. Ind. Electron.*, vol. 71, no. 8, pp. 9460–9469, 2024, doi: 10.1109/TIE.2023.3317840.

[26] X. Zhang and Z. Zheng, "Application of Repetitive Control in Electric Spring," *IEEE Access*, vol. 8, pp. 216607–216616, 2020, doi: 10.1109/ACCESS.2020.3041648.

[27] K. Zhou, C. Tang, Y. Chen, B. Zhang, and W. Lu, "A Generic Multi-Frequency Repetitive Control Scheme for Power Converters," *IEEE Trans. Ind. Electron.*, vol. 70, no. 12, pp. 12680–12688, 2023, doi: 10.1109/TIE.2023.3239855.

[28] W. Lu, W. Wang, K. Zhou, and Q. Fan, "General High-Order Selective Harmonic Repetitive Control for PWM Converters," *IEEE J. Emerg. Sel. Top. Power Electron.*, vol. 10, no. 1, pp. 1178–1191, 2022, doi: 10.1109/JESTPE.2021.3101857.

[29] E. Kurniawan *et al.*, "Design and analysis of higher-order repetitive sliding mode controller for uncertain linear systems with time-varying periodic disturbances," *Trans. Inst. Meas. Control*, vol. 45, no. 12, pp. 2219–2234, 2023, doi: 10.1177/01423312221146604.

[30] G. Ramos, J. M. Olm, and R. Costa-Castelló, "Adaptive Compensation Strategy For The Tracking/Rejection of Signals with Time-Varying Frequency in Digital Repetitive Control Systems," *J. Process Control*, vol. 20, Sep. 2009, doi: 10.1016/j.jprocont.2010.02.002.

[31] E. Kurniawan, H. G. Harno, and H. Adinanta, "High-order repetitive model reference control for linear systems with uncertain periodic references and disturbances," *Int. J. Syst. Sci.*, vol. 53, no. 7, pp. 1456–1468, 2022, doi: 10.1080/00207721.2021.2008545.

[32] C. Verrelli, "Repetitive Learning Control Design and Period Uncertainties," *Asian J. Control*, vol. 17, Mar. 2015, doi: 10.1002/asjc.1125.

[33] M. Steinbuch, S. Weiland, and T. Singh, "Design of noise and period-time robust high-order repetitive control, with application to optical storage," *Automatica*, vol. 43, no. 12, pp. 2086–2095, 2007, doi: 10.1016/j.automatica.2007.04.011.

[34] G. A. Ramos, R. Costa-Castelló, and J. M. Olm, "Odd-harmonic high order repetitive control," *Digital Repetitive Control under Varying Frequency Conditions*, pp. 37-64, 2013, doi: 10.1007/978-3-642-37778-5_5.

[35] R. Chuei and Z. Cao, "Extreme learning machine-based super-twisting repetitive control for aperiodic disturbance, parameter uncertainty, friction, and backlash compensations of a brushless DC servo motor," *Neural Comput. Appl.*, vol. 32, no. 18, pp. 14483–14495, 2020, doi: 10.1007/s00521-020-04965-w.

[36] Z. Zhao, S. Lin, D. Zhu, and G. Wen, "Vibration Control of a Riser-Vessel System Subject to Input Backlash and Extraneous Disturbances," *IEEE Trans. Circuits Syst. II Express Briefs*, vol. 67, no. 3, pp. 516–520, 2020, doi: 10.1109/TCSII.2019.2914061.

[37] W. Lin *et al.*, "Adaptive Extended State Observer-Based Velocity-Free Servo Tracking Control With Friction Compensation," *IEEE Trans. Syst. Man, Cybern. Syst.*, vol. 54, no. 1, pp. 2–11, 2024, doi: 10.1109/TSMC.2023.3299953.

[38] A. H. M. Sayem, Z. Cao, and Z. Man, "Model Free ESO-Based Repetitive Control for Rejecting Periodic and Aperiodic Disturbances," *IEEE Trans. Ind. Electron.*, vol. 64, no. 4, pp. 3433–3441, 2017, doi: 10.1109/TIE.2016.2606086.

[39] M. Nordin and P.-O. Gutman, "Controlling mechanical systems with backlash—a survey," *Automatica*, vol. 38, no. 10, pp. 1633–1649, 2002, doi: 10.1016/S0005-1098(02)00047-X.

[40] M. Çetin, B. Bahtiyar, and S. Beyhan, "Adaptive uncertainty compensation-based nonlinear model predictive control with real-time applications," *Neural Comput. Appl.*, vol. 31, no. 2, pp. 1029–1043, 2019, doi: 10.1007/s00521-017-3068-7.

[41] H. Yan and Y. Li, "Adaptive NN prescribed performance control for nonlinear systems with output dead zone," *Neural Comput. Appl.*, vol. 28, no. 1, pp. 145–153, 2017, doi: 10.1007/s00521-015-2043-4.

[42] İ. Eski and Ş. Yıldırım, "Neural network-based fuzzy inference system for speed control of heavy duty vehicles with electronic throttle control system," *Neural Comput. Appl.*, vol. 28, pp. 907–916, 2017, doi: 10.1007/s00521-016-2362-0.

[43] Q. Li, T. Zhang, G. Li, Z. Li, H. Xia, and C.-Y. Su, "Neural-Dynamics Optimization and Repetitive Learning Control for Robotic Leg Prostheses," *IEEE/ASME Trans. Mechatronics*, vol. 27, no. 2, pp. 811–822, 2022, doi: 10.1109/TMECH.2021.3071936.

[44] V. H. Duenas, C. A. Cousin, C. Rouse, E. J. Fox, and W. E. Dixon, "Distributed Repetitive Learning Control for Cooperative Cadence Tracking in Functional Electrical Stimulation Cycling," *IEEE Trans. Cybern.*, vol. 50, no. 3, pp. 1084–1095, 2020, doi: 10.1109/TCYB.2018.2882755.

[45] M. Yang, Y. Zhang, Z. Zhang, and H. Hu, "6-Step Discrete ZNN Model for Repetitive Motion Control of Redundant Manipulator," *IEEE Trans. Syst. Man, Cybern. Syst.*, vol. 52, no. 8, pp. 4969–4980, 2022, doi: 10.1109/TSMC.2021.3107898.

[46] C. Xu, S. Xie, and Q. Chen, "Neural-network-based adaptive repetitive learning control for a class of non-parametric uncertain systems," *Gaojishu Tongxin/Chinese High Technol. Lett.*, vol. 32, no. 8, pp. 859–865, 2022, doi: 10.3772/j.issn.1002-0470.2022.08.008.

[47] E. Tatlicioglu, N. Cobanoglu, and E. Zergeroglu, "Neural network-based repetitive learning control of euler lagrange systems: An output feedback approach," *IEEE Control Syst. Lett.*, vol. 2, no. 1, pp. 13–18, 2018, doi: 10.1109/LCSYS.2017.2720735.

[48] Z. B. Duranay, "Extreme Learning Machine-Based Power Forecasting in Photovoltaic Systems," *IEEE Access*, vol. 11, pp. 128923–128931, 2023, doi: 10.1109/ACCESS.2023.3333667.

[49] K. Xu, H. Yang, C. Zhu, X. Jin, B. Fan, and L. Hu, "Deep Extreme Learning Machines Based Two-Phase Spatiotemporal Modeling for Distributed Parameter Systems," *IEEE Trans. Ind. Informatics*, vol. 19, no. 3, pp. 2919–2929, 2023, doi: 10.1109/TII.2022.3165870.

[50] H. D. P. De Carvalho, R. Fagundes, and W. Santos, "Extreme Learning Machine Applied to Software Development Effort Estimation," *IEEE Access*, vol. 9, pp. 92676–92687, 2021, doi: 10.1109/ACCESS.2021.3091313.

[51] Z. Wang, Y. Zeng, Y. Liu, and D. Li, "Deep Belief Network Integrating Improved Kernel-Based Extreme Learning Machine for Network Intrusion Detection," *IEEE Access*, vol. 9, pp. 16062–16091, 2021, doi: 10.1109/ACCESS.2021.3051074.

[52] M. Nahiduzzaman *et al.*, "A Novel Method for Multivariant Pneumonia Classification Based on Hybrid CNN-PCA Based Feature Extraction Using Extreme Learning Machine With CXR Images," *IEEE Access*, vol. 9, pp. 147512–147526, 2021, doi: 10.1109/ACCESS.2021.3123782.

[53] R. Alasbahi and X. Zheng, "An Online Transfer Learning Framework With Extreme Learning Machine for Automated Credit Scoring," *IEEE Access*, vol. 10, pp. 46697–46716, 2022, doi: 10.1109/ACCESS.2022.3171569.

[54] J. Li, C. Hai, Z. Feng, and G. Li, "A Transformer Fault Diagnosis Method Based on Parameters Optimization of Hybrid Kernel Extreme Learning Machine," *IEEE Access*, vol. 9, pp. 126891–126902, 2021, doi: 10.1109/ACCESS.2021.3112478.

[55] M. Nahiduzzaman, M. R. Islam, S. M. R. Islam, M. O. F. Goni, M. S. Anower, and K.-S. Kwak, "Hybrid CNN-SVD Based Prominent Feature Extraction and Selection for Grading Diabetic Retinopathy Using Extreme Learning Machine Algorithm," *IEEE Access*, vol. 9, pp. 152261–152274, 2021, doi: 10.1109/ACCESS.2021.3125791.

[56] H. Lin, X. He, S. Wang, and P. Yang, "Wavefront Distortion Correction for the Non-Uniform-Intensity Light Based on Extreme Learning Machine," *IEEE Photonics J.*, vol. 13, no. 3, pp. 1–10, 2021, doi: 10.1109/JPHOT.2021.3086005.

[57] K. Zheng, J. Yang, Q. Gong, S. Zhou, L. Zeng, and S. Li, "Multivariate Extreme Learning Machine Based AutoEncoder for Electricity Consumption Series Clustering," *IEEE Access*, vol. 9, pp. 148665–148675, 2021, doi: 10.1109/ACCESS.2021.3124009.

[58] J. M. Melchor-Leal and J. A. Cantoral-Ceballos, "Force profile characterization for thermostatic bimetal using extreme learning machine," *IEEE Lat. Am. Trans.*, vol. 19, no. 2, pp. 208–216, 2021, doi: 10.1109/TLA.2021.9443062.

[59] P. P. Játiva, R. Becerra, C. A. Azurdia-Meza, D. Zabala-Blanco, I. Soto, and M. R. Cañizares, "Extreme Learning Machine Based Channel Estimator and Equalizer for Underground Mining VLC Systems," in *2021 IEEE Latin-American Conference on Communications (LATINCOM)*, pp. 1–6, 2021, doi: 10.1109/LATINCOM53176.2021.9647737.

[60] F. Luo, G. Liu, W. Guo, G. Chen, and N. Xiong, "ML-KELM: A Kernel Extreme Learning Machine Scheme for Multi-Label Classification of Real Time Data Stream in SIoT," *IEEE Trans. Netw. Sci. Eng.*, vol. 9, no. 3, pp. 1044–1055, 2022, doi: 10.1109/TNSE.2021.3073431.

[61] J. Zhang, H. Wang, M. Ma, M. Yu, A. Yazdani, and L. Chen, "Active Front Steering-Based Electronic Stability Control for Steer-by-Wire Vehicles via Terminal Sliding Mode and Extreme Learning Machine," *IEEE Trans. Veh. Technol.*, vol. 69, no. 12, pp. 14713–14726, 2020, doi: 10.1109/TVT.2020.3036400.

[62] H. Gao, W. Tang, and R. Fu, "Sliding Mode Control for Hypersonic Vehicle Based on Extreme Learning Machine Neural Network Disturbance Observer," *IEEE Access*, vol. 10, no. June, pp. 69333–69345, 2022, doi: 10.1109/ACCESS.2022.3185256.

[63] Y. Yang, Y. Wang, X. Yuan, Y. Chen, and L. Tan, "Neural network-based self-learning control for power transmission line deicing robot," *Neural Comput. Appl.*, vol. 22, no. 5, pp. 969–986, 2013, doi: 10.1007/s00521-011-0789-x.

[64] Z. Wang *et al.*, "Sensor Drift Compensation of E-Nose Systems with Discriminative Domain Reconstruction Based on an Extreme Learning Machine," *IEEE Sens. J.*, vol. 21, no. 15, pp. 17144–17153, 2021, doi: 10.1109/JSEN.2021.3081923.

[65] Y. Zheng, Z. Cao, S. Wang, Z. Man, and R. Chuei, "Extreme learning machine-based field-oriented feedback linearization speed control of permanent magnetic synchronous motors," *Neural Comput. Appl.*, vol. 34, no. 7, pp. 5267–5282, 2022, doi: 10.1007/s00521-021-06722-z.

[66] L. Chen, B. Yan, H. Wang, K. Shao, E. Kurniawan, and G. Wang, "Extreme-learning-machine-based robust integral terminal sliding mode control of bicycle robot," *Control Eng. Pract.*, vol. 121, p. 105064, 2022, doi: 10.1016/j.conengprac.2022.105064.

[67] Y. Hu *et al.*, "Extreme-learning-machine-based FNTSM control strategy for electronic throttle," *Neural Comput. Appl.*, vol. 32, no. 18, pp. 14507–14518, 2020, doi: 10.1007/s00521-019-04446-9.

[68] D. Wu, H. Chen, Y. Huang, and S. Chen, "Online Monitoring and Model-Free Adaptive Control of Weld Penetration in VPPAW Based on Extreme Learning Machine," *IEEE Trans. Ind. Informatics*, vol. 15, no. 5, pp. 2732–2740, 2019, doi: 10.1109/TII.2018.2870933.

[69] H. J. Rong and G. S. Zhao, "Direct adaptive neural control of nonlinear systems with extreme learning machine," *Neural Comput. Appl.*, vol. 22, no. 3–4, pp. 577–586, 2013, doi: 10.1007/s00521-011-0805-1.

[70] C. Yang, K. Huang, H. Cheng, Y. Li, and C. Y. Su, "Haptic Identification by ELM-Controlled Uncertain Manipulator," *IEEE Trans. Syst. Man, Cybern. Syst.*, vol. 47, no. 8, pp. 2398–2409, 2017, doi: 10.1109/TSMC.2017.2676022.

[71] Quanser, *Rotary Experiment 01: SRV02 Modeling using QuaRC*. Markham, Ontario: Quanser Inc., 2011.

[72] Y. Chen, K. Zhou, C. Tang, Y. Shu, and Y. Yang, "Fractional-Order Multiperiodic Odd-Harmonic Repetitive Control of Programmable AC Power Sources," *IEEE Trans. Power Electron.*, vol. 37, no. 7, pp. 7751–7758, 2022, doi: 10.1109/TPEL.2022.3147062.

[73] C. Lin *et al.*, "Output Voltage Ripple Suppression of PPSS-LCC Converter for Medical X-Ray Application Based on Repetitive Control," *IEEE J. Emerg. Sel. Top. Ind. Electron.*, vol. 5, no. 4, pp. 1688–1697, 2024, doi: 10.1109/JESTIE.2024.3435005.

[74] M. S. Ali, L. Wang, H. Alquhayz, O. U. Rehman, and G. Chen, "Performance Improvement of Three-Phase Boost Power Factor Correction Rectifier Through Combined Parameters Optimization of Proportional-Integral and Repetitive Controller," *IEEE Access*, vol. 9, pp. 58893–58909, 2021, doi: 10.1109/ACCESS.2021.3073004.

[75] J. Ye, L. Liu, J. Xu, and A. Shen, "Frequency Adaptive Proportional-Repetitive Control for Grid-Connected Inverters," *IEEE Trans. Ind. Electron.*, vol. 68, no. 9, pp. 7965–7974, 2021, doi: 10.1109/TIE.2020.3016247.

[76] Z. Chen, H. Zha, K. Peng, J. Yang, and J. Yan, "A Design Method of Optimal PID-Based Repetitive Control Systems," *IEEE Access*, vol. 8, pp. 139625–139633, 2020, doi: 10.1109/ACCESS.2020.3012506.

[77] M. Jamil, A. Waris, S. O. Gilani, B. A. Khawaja, M. N. Khan, and A. Raza, "Design of Robust Higher-Order Repetitive Controller Using Phase Lead Compensator," *IEEE Access*, vol. 8, pp. 30603–30614, 2020, doi: 10.1109/ACCESS.2020.2973168.

[78] A. Straś, B. Ufnalski, M. Michalczuk, A. Gałecki, and L. Grzesiak, "Design of fractional delay repetitive control with a dead-beat compensator for a grid-tied converter under distorted grid voltage conditions," *Control Eng. Pract.*, vol. 98, p. 104374, 2020, doi: 10.1016/j.conengprac.2020.104374.

[79] H. Zhou. *Extreme learning machine for classification and regression*. Doctoral thesis, Nanyang Technological University, Singapore, 2013.

[80] G. Bin Huang, Q. Y. Zhu, and C. K. Siew, "Extreme learning machine: Theory and applications," *Neurocomputing*, vol. 70, no. 1–3, pp. 489–501, 2006, doi: 10.1016/j.neucom.2005.12.126.

[81] E. Kurniawan. *Robust Repetitive Control and Applications.* Swinburne University of Technology, Melbourne, Australia, 2013.

[82] G.-B. Huang, L. Chen, and C. Siew, "Universal Approximation Using Incremental Constructive Feedforward Networks With Random Hidden Nodes," *IEEE Trans. Neural Netw.*, vol. 17, pp. 879–892, Jul. 2006, doi: 10.1109/TNN.2006.875977.

[83] W. Cao, J. Gao, Z. Ming, and S. Cai, "Some Tricks in Parameter Selection for Extreme Learning Machine," *IOP Conf. Ser. Mater. Sci. Eng.*, vol. 261, no. 1, p. 12002, 2017, doi: 10.1088/1757-899X/261/1/012002.

[84] L. Hua, C. Zhang, T. Peng, C. Ji, and M. Shahzad Nazir, "Integrated framework of extreme learning machine (ELM) based on improved atom search optimization for short-term wind speed prediction," *Energy Convers. Manag.*, vol. 252, p. 115102, 2022, doi: 10.1016/j.enconman.2021.115102.

[85] X. Zheng and G. Xu, "Extreme learning machine with incremental hidden layers," in *Third International Conference on Electronic Information Engineering, Big Data, and Computer Technology (EIBDCT 2024)*, vol. 13181, pp. 2105-2110, 2024, doi: 10.1117/12.3031279.

[86] C. Y. Lin and C. M. Chang, "Hybrid proportional derivative/repetitive control for active vibration control of smart piezoelectric structures," *JVC/Journal Vib. Control*, vol. 19, no. 7, pp. 992–1003, 2013, doi: 10.1177/1077546312436749.